The 2010 IEEE/RSJ International Conference on
Intelligent Robots and Systems
October 18-22, 2010, Taipei, Taiwan

Three-Dimensional Visualization of Photoelastic Stress Analysis for Catheter Insertion Robot

Motoki Matsushima, Carlos R. Tercero, *Member, IEEE*, Seiichi Ikeda, *Member, IEEE*, Toshio Fukuda, *Fellow, IEEE*, and Makoto Negoro

***Abstract*— It is desirable for endovascular surgery simulation to describe with quantitative data the interaction between the catheter and the blood vessel model wall to make an objective evaluation of the procedure. Photoelastic stress analysis in straight segments of multi-layered models was used for that purpose. In this research we study the error introduced by stress direction on the magnitude measurements, for photoelastic stress analysis. And we propose a scanner for three dimensional visualization of photoelastic stress analysis. As result, we quantified that the maximum contribution of error from stress direction in the first half of the fringe is 2.52% for the stress magnitude measurements. Three-dimensional stress visualization was obtained in segment of straight vasculature with an average error in sample slices of 10.73%, 4.55% and 3.18% for inner pressures of 80, 120 and 160mmHg respectively.**

I. Introduction

SILICONE models of vasculature were developed for endovascular surgery simulation as they can reproduce lumen of human vasculature with 13μm of accuracy and membranous tissue as well [1]. Integration of multiple sections of vasculature enables practice of endovascular procedures and evaluation of catheter insertion robots [2], Fig.1. However it is necessary to develop measurement methods to quantify the interaction between the catheters or guide wires and the blood vessel models to evaluate the person or robot driving the catheter, and also to compare the performance between different catheter types.

Polarized light undergoes a phase shift when passing through photoelastic materials producing birefringence. The resulting phase shift is called retardation and its variation is described by equation (1) for a two-dimensional stress analysis:

$$\sigma_1 - \sigma_2 = \frac{\mathrm{Re}}{cD} \tag{1}$$

Where *Re* is the retardation and is measured in nanometers, D is the optical path length (thickness of the photoelastic material), *c* is the photoelastic coefficient and σ_1, σ_2 are the principal stresses on each side of a biaxial stress field [3].

Manuscript received March 10, 2010. This work was supported in part by the Global Centers of Excellence program of Nagoya University and in part by Grants-in-Aid for Scientific Research of the Japan Society of Promotion of Science. M. Matsushima, C. R. Tercero, S. Ikeda, and T. Fukuda are with the Department of Micro-Nano Systems Engineering, Nagoya University, Nagoya 464-8603, Japan (e-mail: matsushima@robo.mein.nagoya-uac.jp; tercero@robo.mein.nagoya-u.ac.jp; ikeda@robo.mein.nagoya-u.ac.jp; fukuda@robo.mein.nagoya-u.ac.jp). M. Negoro is with the Department of Neurosurgery, Fujita Health University, Toyoake 470-1192, Japan (e-mail: mnegoro@fujita-hu.ac.jp).

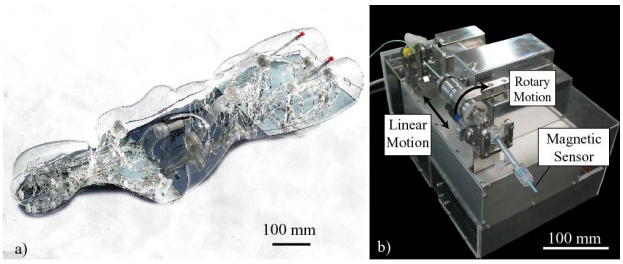

Fig. 1: a) Endovascular Surgery Simulation System. b) Robot for autonomous catheter insertion path reconstruction.

Photoelastic effect has been used for evaluation of strain in ligaments and femoral surface [4-5]. Single layer models of urethane elastomer and photoelastic effect were used in [6] to measure the effect of micro-coils insertion on catheter tip in the catheter performance. Urethane elastomer is a birefringent material that enables stress field visualization under polarized light. Multilayer models of straight segments of vasculature were presented in [7-8]; a urethane elastomer layer was shielded by two layers of silicone elastomer. This enabled visualization of human blood pressure simulation in [7], and quantification of the photoelastic stress measurement average error in a straight segment of vasculature for inner pressures of 60-189mmHg at 3.9% [8]. Thus with photoelastic effect, commercially available intravascular tools do not need to be modified to evaluate the interaction between them and phantom membrane.

When the polarizer shown in figure 2 is used, retardation in multi-layered blood vessel models relates with perceived green light intensity by:

$$I_{GN} = \sin^2\frac{\pi\,\mathrm{Re}}{\lambda_G}\left(\cos^2(2\theta)\sin^2\left(\frac{\lambda_{ex}\pi}{2\lambda_G}\right)+\sin^2(2\theta)\right) \tag{2}$$

Where I_{GN} is the normalized green light intensity, θ is the stress direction; λ_{ex} and λ_G are the wavelengths of the quarter plates and the perceived green light and are measured in nanometers [8, 9]. To evaluate more precisely the interaction of the catheter, guide wire, stents and coils it is desirable to have a three-dimensional image of the stress distribution. In this research, we quantified the contribution of stress direction in stress magnitude measurements using the polariscope described by (2); also we propose a scanner for capturing the sinogram of a blood vessel model slice, and achieve a three-dimensional visualization of stress distribution by reconstructing each slice using the Maximum Likelihood – Expectation Maximization (ML-EM) Method [10].

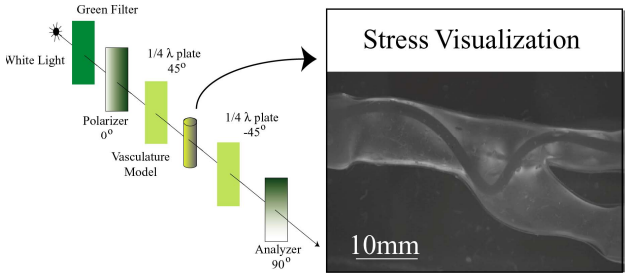

Fig. 2: Polarizer minimizing effect of stress direction in stress magnitude measurements using photoelastic effect (Left) Retardation of polarized light by stress in multilayered model of carotid artery.

II. Materials And Methods

A. Stress Analysis in borders of pipe

For the three dimensional stress analysis described in [11], retardation relates with stress components by equation (3)

$$\left(\frac{\mathrm{Re}}{cD}\right)^2 = \begin{bmatrix} \left(1-v_1^2\right)^2\left(\sigma_1-\sigma_2\right)^2 \\ +\left(1-v_3^2\right)^2\left(\sigma_2-\sigma_3\right)^2 \\ +2\left(v_2^2-v_3^2v_1^2\right)^2\left(\sigma_1-\sigma_2\right)\left(\sigma_2-\sigma_3\right) \end{bmatrix} \quad (3)$$

where v_1, v_2, and v_3 are the magnitudes for the unitary vectors that describe the light beam direction in terms of the principal stresses σ_1, σ_2 and the radial stress component σ_3. Equation (1) is obtained when the light beam is parallel to σ_3, v_1=v_2=0 and v_3 =1. When the principal stress plane is parallel to the light beam, v_1=-cosφ, v_2 = sinφ, and v_3 =0, then:

$$\left(\frac{\mathrm{Re}}{cD}\right)^2 = \begin{bmatrix} \left(1-\cos^2\varphi\right)^2\left(\sigma_1-\sigma_2\right)^2 \\ +\left(\sigma_2-\sigma_3\right)^2 \\ +2\sin^2\varphi\left(\sigma_1-\sigma_2\right)\left(\sigma_2-\sigma_3\right) \end{bmatrix} \quad (4)$$

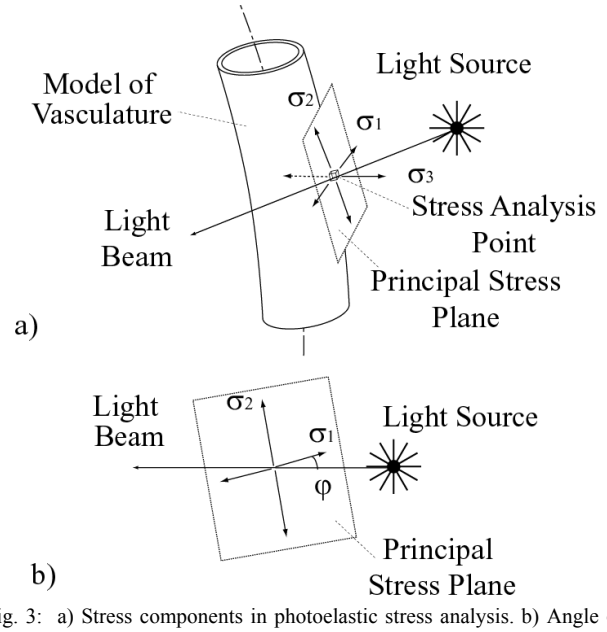

Fig. 3: a) Stress components in photoelastic stress analysis. b) Angle φ between principal stress component σ_2 and light beam (Right).

where φ is the angle between the light beam and σ_1, Fig. 3. And if the radial stress component σ_3 is considered zero; the equation (4) is reduced to:

$$\frac{\mathrm{Re}}{cD} = \left(\sigma_1\sin^2\varphi + \sigma_2\cos^2\varphi\right) \quad (5)$$

For this research we consider that the model of vasculature has cylindrical shape, and we set its axis perpendicular to the light source beam. Therefore in this case equation (5) can be reduced to:

$$\frac{\mathrm{Re}}{cD} = \sigma_2 \quad (6)$$

B. Stress Direction Contribution on Stress Magnitude Measurement Error

For models of vasculature θ is the direction of the projection of σ_2 in the polarizer plane, it is desirable to quantify its contribution into the stress magnitude measurements to support the simplification of (2) into

$$I_{GN} \approx \sin^2\left(\frac{\pi\,\mathrm{Re}}{\lambda_G}\right) \quad (7)$$

For that purpose we placed a variable retardation device inside the polarizer of figure 2. This device is composed of stacked quarter-wave plates oriented in the same direction, and providing retardation zones of 0, 140, 280, 420 and 560nm. Changing the orientation of the variable retardation device inside the polarizer and measuring the green light intensity at each zone enables us to study the effect of θ in the measurement of *Re*. Green light intensity measurements were done in each zone for the orientation range 0-180 degrees in 15 degrees intervals.

C. ML-EM Method

The sinogram is an image where each row represents a direction, and each column a spatial coordinate of the studied cross-section. ML-EM is an iterative method that reconstructs the cross-section of the observed object using the sinogram (forward projection) of a slice of the object, Fig.4. Let's consider B^k the result image of the reconstruction process at iteration k and C^k the sinogram of B^k. B^0 is the image of an object with square cross-section, Fig. 5. D^k is the division pixel by pixel between images A and C^k, E^k is normalized back projection of D^k, and B^{k+1} is obtained from the multiplication between E^k and B^k. The reconstruction of a pipe cross-section after one and twenty iterations is shown on fig.6.

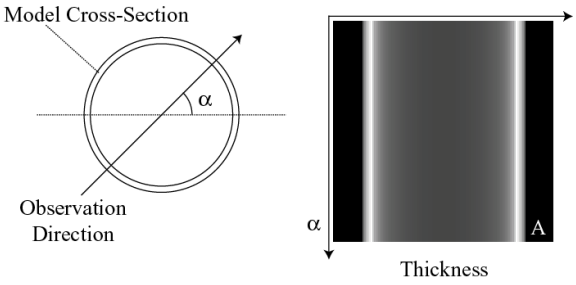

Fig. 4: Blood vessel model slice (Left) and its corresponding sinogram: Image *A* (Right).

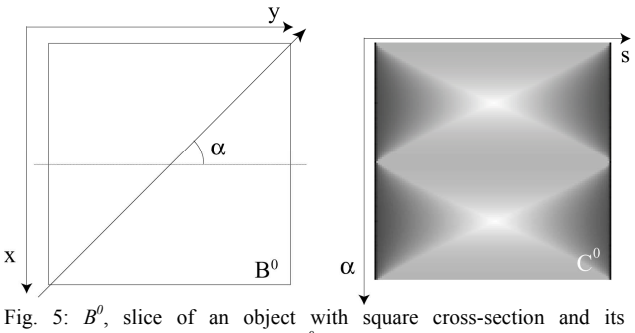

Fig. 5: B^0, slice of an object with square cross-section and its corresponding sinogram is image C^0.

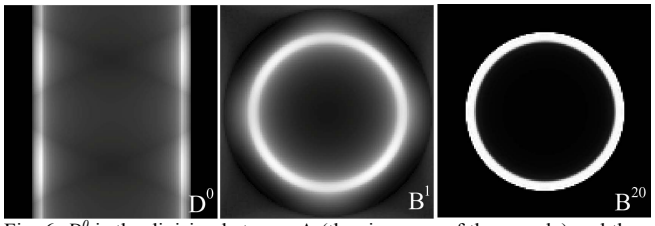

Fig. 6: D^0 is the division between A (the sinogram of the sample) and the sinogram of the first approximation C^0. B^1 and B^{20} are the result of iterations one and twenty.

D. Scanner for three dimensional visualization of photoelastic stress analysis

The polarizer of figure 2 and a camera were attached to a glycerine tank. This structure has its rotation axis inside the tank, enabling to scan in 360 degrees the phantom submerged into the tank by capturing images with the camera, Fig. 7. A multi-layered model simulating a straight segment of vasculature was submerged into the tank, concentric to the rotation axis. Pressure inside the model was set at three levels along the range defined in [8]; P_1=80mmHg, P_2=120mmHg and P_3=160mmHg. For each pressure two sets of images were recorded: first scan was performed with a blue filter instead of the polarizer to obtain 128 source images in a range of 180 degrees. Those images were used for the sinograms construction for each pressure and slice, the sinogram $A^n{}_p$ corresponds to slice n at pressure P. Then optical path length was calculated for each sinogram. Second scan was done with the polarizer in place for the same directions to register the green light retardation. From them, the sinogram $R^n{}_p$ of slice n at pressure P were built for each pressure and slice.

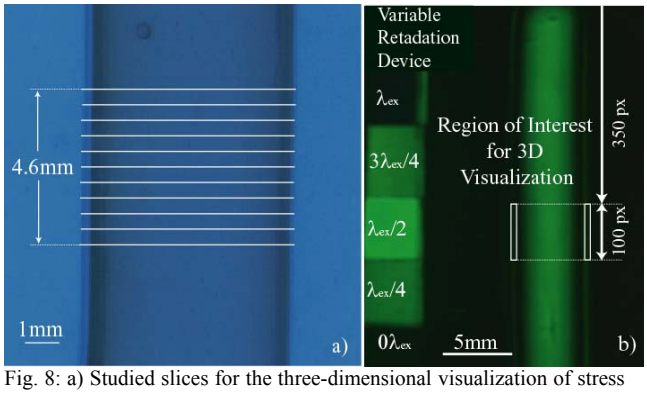

Fig. 8: a) Studied slices for the three-dimensional visualization of stress over a source image sample for optical path length calculation. b) Retardation of green light produced by stress in the model wall.

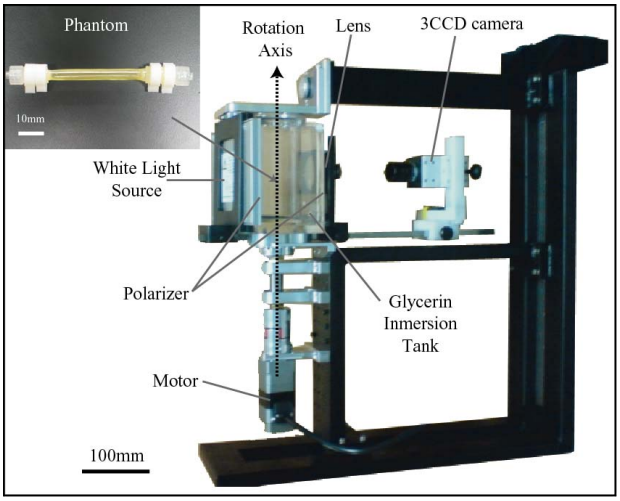

Fig.7: Scanner for building the sinogram of each slice of the model of vasculature submerged into the glycerin tank.

For each image the region of interest is limited to the borders of the model from rows 350 to 449 as illustrated in figure 8.

Longitudinal stress varies in a cylinder according to [12]:

$$\sigma_2 = \frac{(r-t)^2}{r^2-(r-t)^2} P_{in} \tag{8}$$

where P_{in} is the pressure inside the cylinder, r is the cylinder radius and t the wall thickness. For evaluating the accuracy of the system this model is used to describe the stress on the edge of the blood vessel model.

E. Application of EL-EM Method to Photoelastic Stress Measurements

$A^n{}_p$ images were used as source for reconstructing 10 slices of the thickness of the blood vessel model following the method described in section II.C. However for reconstructing the stress distribution from $R^n{}_p$, some modifications of the ML-EM method explained above were done.

$B^{n,20}{}_p$ is the reconstructed image of slice n at pressure P after twenty iterations. In that grey scale image, white represent the model presence and black the absence. A threshold level was applied to set to zero the pixels with a value below 128, and set to 255 those with a value above. The resulting image $B'^{n,0}$ is used as the first approximation to apply the ML-EM method to reconstruct the stress distribution.

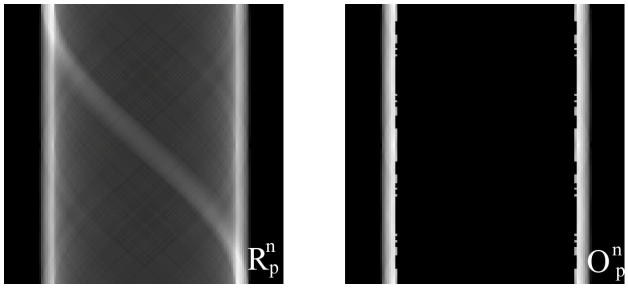

Fig. 9: Images $R^n{}_p$ and $O^n{}_p$ are the sinogram of the retardation and the region of interest extraction for the slice n at pressure P

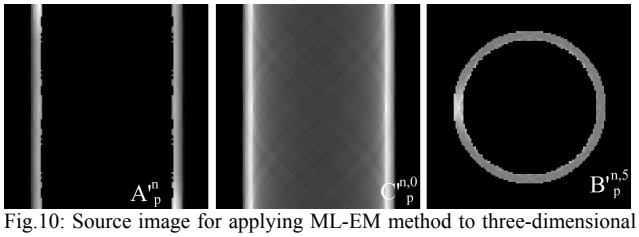

Fig.10: Source image for applying ML-EM method to three-dimensional visualization of stress A'^{n}_{p}. $C'^{n,0}$, sinogram of $B'^{n,0}$. $B'^{n,0}$ is the result of average stress reconstruction in a slice after 5 iterations.

The optical path length at the region of interest O^{n}_{p} was extracted from the sinograms A^{n}_{p}, the external wall location $L_{o\alpha}$ was identified when thickness reaches 1200μm and the inner wall location $L_{i\alpha}$ when the maximum thickness is reached. After that the average stress S^{n}_{p} must be calculated for the region of interest at each row from the sinogram of retardation and R^{n}_{p} and O^{n}_{p} by:

$$S^{n,a}_{p} = \sum_{s=L_{o\alpha}}^{L_{i\alpha}} \frac{R^{n,a,s}_{p} / cO^{n,a,s}_{p}}{L_{i\alpha} - L_{o\alpha}} \qquad (9)$$

where α is a row of R^{n}_{p} and O^{n}_{p}, s is a column number comprised between the model boundaries. Other pixels were set as zero. Finally image A'^{n}_{p} is calculated by multiplying the sinogram of $B'^{n,0}$ (named $C'^{n,0}$) and S^{n}_{p}. Then the method explained in section II.C was applied to images A'^{n}_{p} and $B'^{n,0}$, after 5 iterations a slice of average stress was reconstructed $B'^{n,5}$, Figs. 9-11. During the application of the ML-EM method if a pixel value of A'^{n}_{p} or $B'^{n,0}$ is zero, the detection probability was brought to zero for that pixel.

III. Results

A. Stress Direction Contribution on Stress Magnitude Measurement Error

The measured green light wave length was λ_G=510nm, the quarter-wave plates provide a retardation of λ_{ex}=140nm with 10nm accuracy. Therefore equation (2) reduces to:

$$I_{GN} = \sin^2 \frac{\pi \,\mathrm{Re}}{510}\left(0.976 + 0.024 \sin^2(2\theta)\right) \qquad (10)$$

The variation of green light intensity with the direction of the variable retardation device is shown on figure 12. Equation (10) forecasts a maximum contribution of 2.4% of the device direction to the intensity measurements. The maximum experimental contribution was observed when retardation is 280nm were the 2.52% was reached. For contributions for 0nm and 140nm were 0% and 1.93% respectively.

B. Source Images Capture and Three-dimensional visualization of stress

Using the scanner shown in figure 7, optical path length and retardation images were captured for the slices within the region of interest at 128 different directions for pressures of 80, 120 and 160mmHg. When the model had an inner pressure of 80mmHG, an additional set of images was captured when a guide wire was inserted.

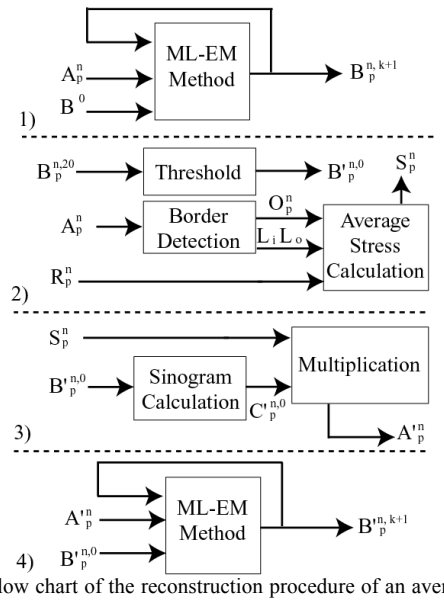

Fig. 11: Flow chart of the reconstruction procedure of an average stress slice

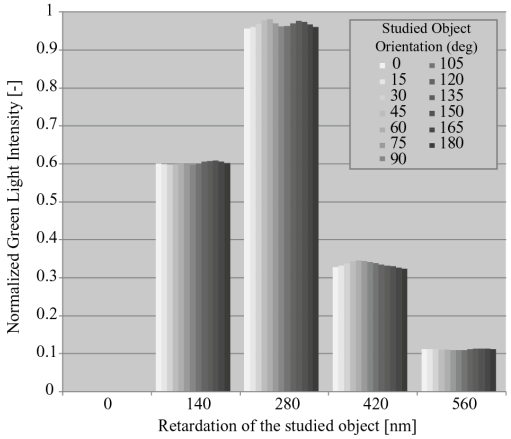

Fig. 12: Variation of green light intensity with the direction of quarter-wave plates.

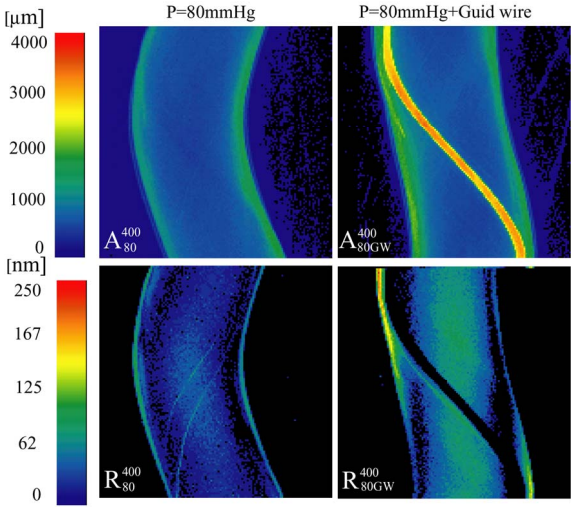

Fig.13: Sinograms of Optical Path Length and Retardation with 80mmHg of pressure inside the model (Left), and with guide wire inserted (Right).

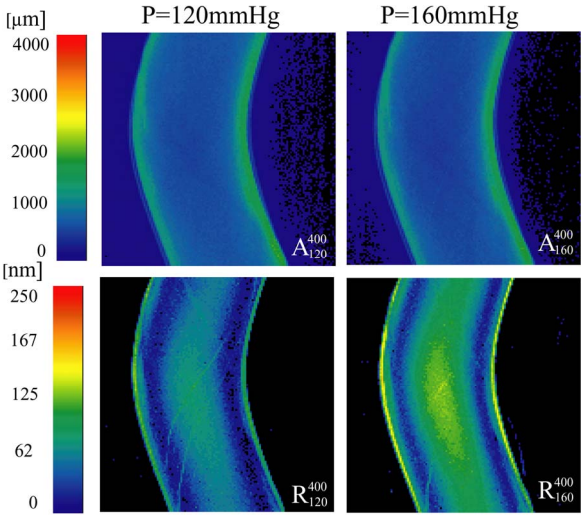

Fig.14: Sinograms of Optical Path Length and Retardation with pressures of 120mmHgl (Left), and 160mmHg (Right).

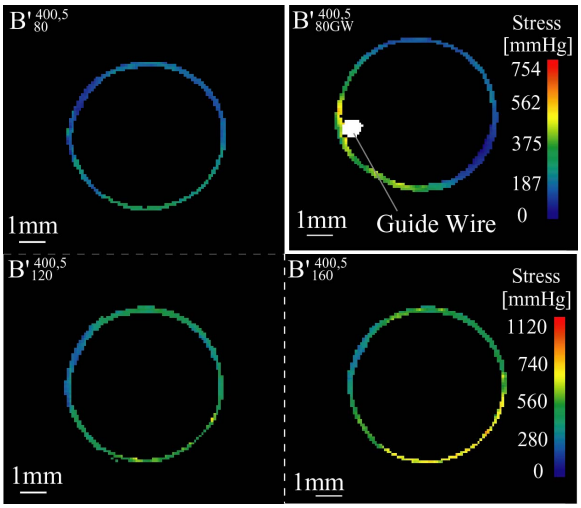

Fig. 15: Reconstruction stress distribution slices using EL-EM method in a model of vasculature slice at pressures of 80,120 and 160mmHg, and with guide wire inserted at 80mmHg.

The resulting sinograms of slice 400 are shown for the four samples in figures 13 and 14. Slices of average stress corresponding to them were reconstructed using the method presented in sections II.C and II.D are show in figure 15. Ten stress distribution slices within the region of interest were loaded to the *Volume Viewer* of *ImageJ* to display the three-dimensional visualization of stress. Figure 16 shows three dimensional views of the blood vessel model with inner pressure of 120mmHg and figure 17 shows views of a model with a guide wire applying stress to the wall and with an inner pressure of 80mmHg. Stress measurement error of images $B'^{400,5}_{80}$, $B'^{400,5}_{120}$, and $B'^{400,5}_{160}$ is of 10.73%, 4.55% and 3.18% respectively, measurements are compared to the mathematical model in figure 18.

IV. Discussion

Stress direction contributed in a maximum of 2.52%, the theory value of the contribution is 2.4%. The difference between them may be caused by the λ_G measurement accuracy and the manufacturing accuracy of the quarter-wave plates. This confirms the usefulness of the approximation of equation (10) to:

$$I_{GN} \approx \sin^2\left(\frac{\pi \,\mathrm{Re}}{510}\right) \tag{11}$$

Slices of stress produced by a guide wire and inner pressure on a blood vessel model were reconstructed and three-dimensionally visualized, however for this experimental setup and measurement accuracy the lumen cross-section diameter of the model is limited to 11.8mm.

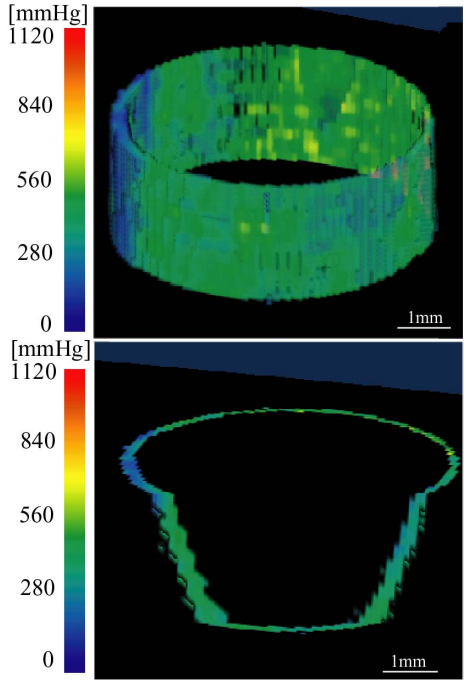

Fig. 16: Three-dimensional visualization of stress for a blood vessel model with inner pressure of 120mmHg.

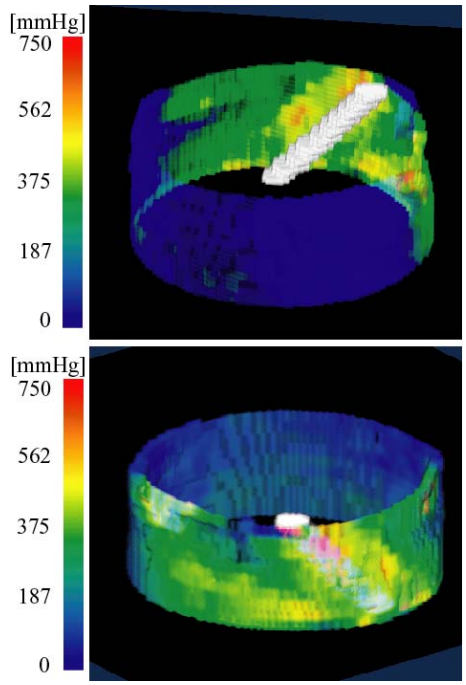

Fig. 17: Three-dimensional visualization of stress for a blood vessel model with inner pressure of 80mmHg and a guide wire inserted.

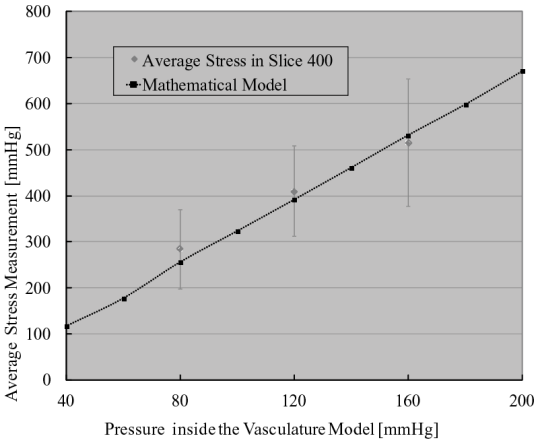

Fig. 17: Variation of stress measurement accuracy for slice 400 with pressure.

Image sizes of the reconstruction method described in II.C and II.E are limited to powers of 2; for this case images of 128x128 pixels were used. The model lumen limit and measurement accuracy depend on the camera resolution and the size of the blood vessel model on the screen. The complete cross-section of the model must appear into the image to be reconstructed properly and it is desirable to maximize the number of pixels belonging to the model wall. The membrane thickness must be at least of three pixels to achieve the accuracy shown in figure 18. However increasing resolution implies increasing the time required to reconstruct each slice and produce the three-dimensional visualization. The large dispersion of error shown in figure 18 may be caused by external forces transmitted to the model during the camera rotation and or low resolution.

Three-dimensional stress visualization is necessary in endovascular surgery simulation for observation and measurement of stress distribution change in blood vessel model wall during human blood pressure simulation, training and evaluation of catheter, stents and coils. Sustain high processing speed and accuracy is an issue that must be tackled to use the proposed system for feedback control of the catheter insertion robot; however it is useful to analyze and compare the stress at some localized spots of the trajectory or to compare different kind of catheters.

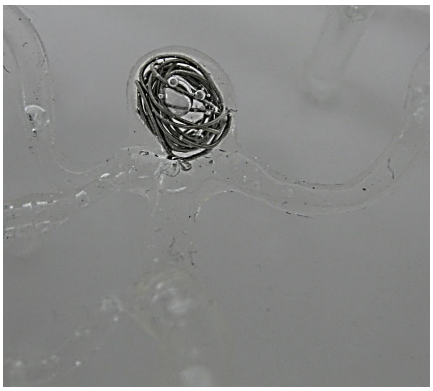

Fig. 19: Coil placement treatment simulation in silicone model of aneurysm.

For placing a stent into a blood vessel it is crucial to select the adequate diameter and length as well for coil placement into aneurysms it is the amount of the aneurysm volume to be filled with coils to avoid rupture and minimize the flow entering to the diseased vasculature, fig. 19. From the results obtained in this research, differentiation between model wall and guide wire was possible during the three-dimensional stress visualization. Therefore stress produced by different kind of coils or stents in a specific morphology of blood vessels can be compared quantitatively. This provides a selection criterion for choosing the best tool for specific treatment and morphology.

V. Conclusion

Three-dimensional stress visualization of the interaction between a guide wire and a straight model of vasculature with inner pressure of 80mmHg was achieved. Slices of the stress distribution were reconstructed using the EL-EM method with average errors of 10.73%, 4.55% and 3.18% for pressures of 80,120 and 160mmHg. As next research step we propose to apply the presented methodology to different blood vessel morphologies and types of stents or coils. At the actual state, this imaging system can be used for off-line quantitative evaluation of human or robot for intravascular tools placement and deployment tasks. However to analyze complete trajectories, image registering speed should be increased.

References

[1] S. Ikeda, F. Arai, T. Fukuda, M. Negoro, and K. Irie, "An in vitro patient specific biological model of the cerebral artery reproduced with a membranous configuration for simulating endovascular intervention," *J.Robot. Mechatronics*, vol. 17, no. 3, pp. 327–333, 2005

[2] C. Tercero, S. Ikeda, T. Uchiyama, T. Fukuda, F. Arai, Y. Okada, Y. Ono, R. Hattori, T. Yamamoto, M. Negoro, I. Takahashi. "Autonomous Catheter Insertion System using Magnetic Motion Capture Sensor for endovascular surgery," International Journal of Medical Robotics and Computer Assisted Surgery. Vol. 3:1 pp 52-58, 2007.

[3] A. Kuske and G. Robertson, *Photoelastic Stress Analysis*. NewYork: Wiley-Interscience, 1974.

[4] S. Hirokawa, K. Yamamoto, and T. Kawada, "A photoelastic study of ligament strain," *IEEE Trans. Rehabil. Eng.*, vol. 6, no. 3, pp. 300–308, Sep. 1998.

[5] M.Grecula, R. Morris, J. Laughlin,W. Buford, and R. Patterson, "Femoral surface strain in intact composite femurs," *IEEE Trans. Biomed. Eng.*, vol. 47, no. 7, pp. 926–933, Jul. 2000.

[6] C. Tercero, Y. Okada, S. Ikeda, T. Fukuda *et al.*, "Numerical evaluation method for catheter prototypes using photo-elastic stress analysis on patient-specific vascular model," *Int. J. Med. Robot. Comput. Assist. Surg.*, vol. 3, no. 4, pp. 349–354, 2007.

[7] C. Tercero, S. Ikeda, E. Tijerino, M. Matsushima, T. Fukuda *et al.*, Human blood pressure simulation for stress analysis in model of vasculature using photoelastic effect," *Int. J. Autom. Technol.*, vol. 3, no. 5, pp. 533–540, 2009.

[8] C. Tercero, S. Ikeda, M. Matsushima, T. Fukuda, M. Negoro. " Photoelastic Stress Analysis Error Quantification in Vasculature Models for Robot Feedback Control," IEEE Trans. on Mechatronics, in press.

[9] D. Goldstein, *Polarized Light*. New York:Marcel Dekker, 2003, ch. 11.

[10] T. Hashimoto e t al., *C Gengo ni yoru Gazou Saikousei no Kiso*. Tokyo: Iryo Kagaku-sya, 2006.

[11] J. Tuji et al., *Koudansei Jikkenhou*. Tokyo: Nikkan Kougyou Shinbun-sya,1965.

[12] H. Li and D. Pugh, *Mechanical Behavior of Materials Under Pressure*. Amsterdam, The Netherlands: Elsevier, 1970, ch. 2.